*Sensors and Materials*, Vol. 30, No. 3 (2018) 347–354
MYU Tokyo



S & M 1496

# Novel Thermal Convection Inclinometer

Jium-Ming Lin[1,2*] and Cheng-Hung Lin[2]

[1]Department of Electronic Engineering, Chung-Hua University,
707, Sec. 2 Wu-Fu Rd., Hsin-Chu, 30012, Taiwan
[2]Ph.D. Program in Engineering Science, Chung-Hua University,
707, Sec. 2 Wu-Fu Rd., Hsin-Chu, 30012, Taiwan

(Received July 3, 2017; accepted October 20, 2017)

***Keywords***: thermal convection, inclinometer, xenon gas, thermal sensor, grooved cavity

In this research, we applied several new ideas for a novel thermal convection inclinometer design. (1) A flexible polyimide (PI) substrate was used instead of a silicon wafer so that the new design can reduce the energy loss of the heater to the substrate. (2) Both the heater and thermal sensors were formed directly on the PI substrate without floating over a grooved cavity on a silicon wafer so that the device is more reliable and cheaper. (3) Inert xenon gas was filled into a hemicylindrical chamber instead of the traditional $CO_2$ gas in a rectangular one, so that we could not only increase the device sensitivity but reduce the oxidation effect. (4) A stacked layer of aluminum nitride was inserted under each thermal sensor to increase the device sensitivity. A prototype device was made to prove the performance of the new design.

## 1. Introduction

Conventional thermal convection accelerometers are manufactured on silicon wafers,[1–4] and the chambers are filled with gases such as nitrogen, argon, $SF_6$, $C_2F_6$, $C_3F_8$, $C_4F_8$, air, and $CO_2$.[5] However, the gases with fluoride would be decomposed by heating and harm the environment. A method of coating a layer of the polyimide (PI) PI-2611 on the silicon was proposed. This method can reduce the power leakage through the silicon substrate previously applied,[6,7] but this design applies either air or $CO_2$ as the convective gas in the chamber, which may not only oxidize but reduce the lifespan of the heater and thermal sensors.[8]

The major idea in this paper is the fabrication of a thermal convection inclinometer on a flexible substrate, such as engineering PI tape,[9] which is much cheaper than a silicon wafer. Since the thermal conductivity of the PI [0.06–0.0017 W/(cm·K)] is about one-twenty-fifth that of silicon [1.48 W/(cm·K)], the use of the PI can considerably reduce the energy leakage out to the substrate.[10] Some studies showed that the sensitivity of the accelerometer can be increased by using a nonfloating structure on a flexible substrate without a grooved cavity when using a conventional silicon-based device.[11–14] Besides, the thermal sensors were stacked on a layer of aluminum nitride (of 1 mm thickness). Moreover, the chamber was filled with an inert gas (xenon) instead of $CO_2$ or air to avoid the component oxidizing effect.[15,16] Thus, both the reliability

*Corresponding author: e-mail: jmlin@chu.edu.tw
http://dx.doi.org/10.18494/SAM.2018.1750

ISSN 0914-4935 © MYU K.K.

and life cycle of the accelerometer could be improved. On the other hand, the hemicylindrical chamber caused the sensitivity to be higher than that with the traditional rectangular chamber.[16–21]

Thus, the above-described new ideas were applied in our study to fabricate a thermal convection inclinometer. Firstly, using the commercial computational fluid dynamics solver (Computational Fluid Dynamics, ESI CFD-ACE+) one could determine a better spacing distance ($D$) between the heater and the thermal sensors. At first, the device was studied with no stacked layer under the thermal sensors. When the inclination angle ($\theta$) was smaller than 60°, the sensitivity curve should be an ideal sinusoid; but when $\theta$ was larger than 60°, the sensitivity curve cannot match the ideal sinusoid. To solve this problem, in this work, we used a layer of aluminum nitride stacked under each thermal sensor, and then the whole sensitivity curve became a sinusoid. The reason for introducing the aluminum nitride was that its thermal conductivity [1.6–3.2 W/(cm·K)] is comparable to that of a copper conductor [4 W/(cm·K)], and its coefficient of thermal expansion ($4.6 \times 10^{-6}$/K) is much lower than that of $SiO_2$ ($8.5 \times 10^{-5}$/K); thus, the thermal convective flow in the chamber would be better. Furthermore, it could reduce the thermal stress at the junctions under the thermal sensors, so the device reliability could be preserved. Two devices with hemicylindrical and rectangular chambers were made and fixed on acrylic substrates covered by PI tape; we found that the sensitivity was better with the new improvements to the hemicylindrical chamber, xenon gas, and the stacked layer of aluminum nitride. This paper is organized as follows. Section 1 is the introduction. Section 2 concerns simulations, such as the trade-off of both the separation distance $D$ of the heater and thermal sensors and the stackness of aluminum nitride. Section 3 concerns the testing of practical devices. Section 4 is the conclusion.

## 2. Simulations and Discussion

ESI CFD-ACE+ was used for the simulation. Figures 1(a) and 1(b) respectively show the side views and parameters of the hemicylindrical and rectangular chambers. The thicknesses of heater and thermal sensors were set as 0.3 mm. The chamber was filled with xenon gas. The thermal sensors applied a p-type semiconductor without any stacked layers at first.

The temperatures of the environment and the heater were respectively set as 300 and 373.15 K.[18–21] To improve the sensitivity, in the following section, we discuss the trade-off among structures, factors, and parameters of devices, such as (1) separation distance $D$, (2) types of chambers, (3) types of filling gases, and (4) thickness and material of stacked layers.

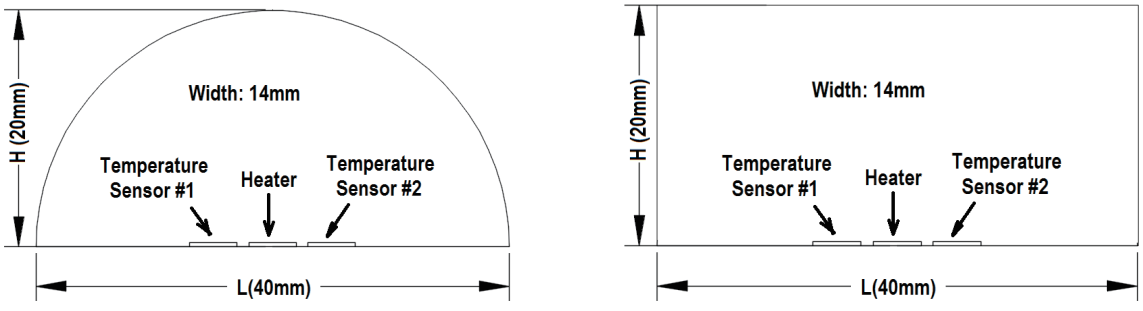


Fig. 1. Side views of devices using (a) hemicylindrical chamber and (b) rectangular chamber.

### 2.1 No stacked layers under thermal sensors

Firstly, we vary the separation distance $D$ without any stacked layers under the thermal sensors. If the device was inclined, the unbalanced thermal convective flow in the chamber would cause a temperature difference between the thermal sensors. The separation distance $D$ was divided into three values (1, 1.25, and 1.5 mm). Figure 2 shows the results of the simulations of sensitivity curves using xenon gas to fill the chambers, in which the results using the hemicylindrical and rectangular chambers were labeled as $H$ and $D$, respectively. Note that when the inclination angle ($\theta$) was smaller than 60°, the sensitivity curves were ideal sinusoids, but when $\theta$ was larger than 60°, the sensitivities were lower than that of the true sinusoid.

The ideal sinusoidal formula to fit the relationships between $\Delta T$ and $\theta$ in Fig. 2 was found to be

$$\Delta T = K \times \sin(\theta). \tag{1}$$

In Eq. (1), $\Delta T$ is the temperature difference, $\theta$ is the inclination angle (0–90°), and $K$ is a proportionality constant. The values of $D$ and $K$ for each type of chamber are listed in Table 1 for comparison. Thus, the case of using the lowest $D$ (= 1 mm) and hemicylindrical chamber was the best, because the thermal convection of the filling gas in the chamber was more streamlined without the reflection effect produced by the rectangular chamber. Secondly, we exchanged the chamber types and filling gases (such as $CO_2$, xenon, $C_4F_8$, and air). The separation distance $D$ was set as 1 mm in accordance with the previous result shown in Fig. 2. Figure 3 shows the sensitivity curves for different types of chambers and gases for comparison. Note that the sensitivity curves using $C_4F_8$ were always the largest, but $C_4F_8$ contains fluoride,

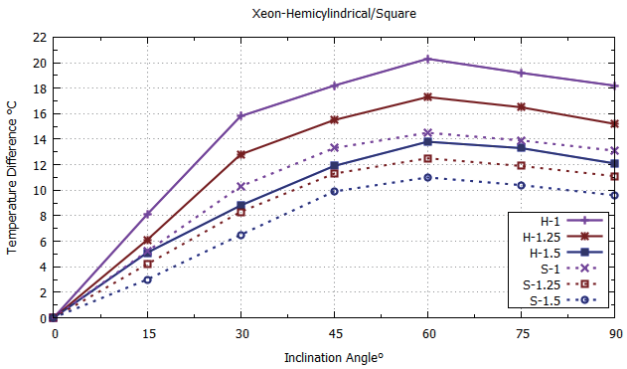


Fig. 2. (Color online) Simulation results of sensitivity curves using different chamber types and separation distances $D$ (1, 1.25, and 1.5 mm).

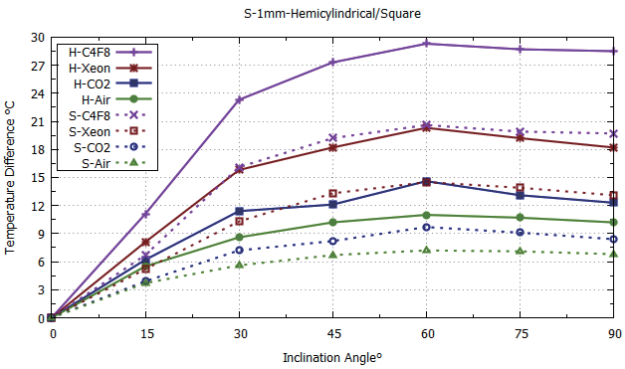


Fig. 3. (Color online) Simulation results of sensitivity curves for hemicylindrical and rectangular chambers with different gases.

Table 1
Values of $K$ for different chambers and separation distances $D$.

| $D$ (mm) | Hemicylindrical chamber | Rectangular chamber |
|---|---|---|
| 1 | 18.2 | 13.1 |
| 1.25 | 15.2 | 12.1 |
| 1.5 | 12.1 | 9.6 |

which harms the ozone layer, so it was discarded in this study. We could also see that the sensitivity curves depend on the molecular weight of the filling gas, because in general, the greater the molecular weight (inertia) of the gas, the higher the sensitivity. These results matched the molecular weights of $C_4F_8$, xenon, $CO_2$ and air, i.e., 220.04, 131.2, 44.01, and 29 g/mol, respectively.

### 2.2 With stacked layers under thermal sensors

Figure 4 shows the device with stacked layers ($W2$). Figures 5 and 6 respectively show the sensitivity curves with $CO_2$ and xenon gases in a hemicylindrical chamber with different values of $W2$ (1, 1.5, 1.8, 2, and 2.3 mm). Note that only the cases with $W2$ = 2.3 mm exhibited ideal sinusoids. Although the use of the stacked layer could solve the one-to-one matching problem between $\Delta T$ and $\theta$, the thickness should be carefully tuned.

## 3. Practical Inclinometer Tests

### 3.1 Inclinometer implementation

Figures 7(a) and 7(b) respectively show the appearance of the devices with hemicylindrical and rectangular chambers. Figure 8 shows that engineering PI tape could be attached to the acrylic substrate to prevent the latter from being melted by the heater. Then a heater wire [Cr (80%)-Ni (20%)] and K-type thermocouples were fixed on the PI tape, as shown in Fig. 9.

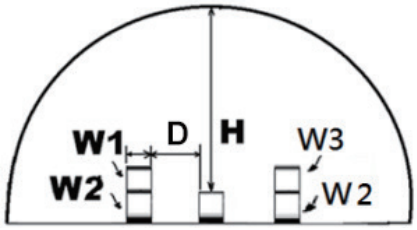


Fig. 4. Proposed devices with stacked layers of aluminum nitride under thermal sensors.

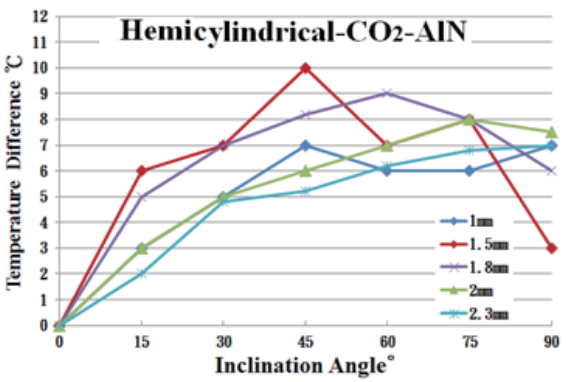


Fig. 5. (Color online) Sensitivity curves with $CO_2$ in a hemicylindrical chamber with different $W2$ values.

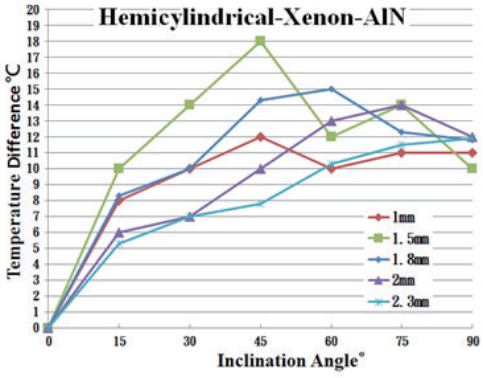


Fig. 6. (Color online) Sensitivity curves with xenon gas in a hemicylindrical chamber with different $W2$ values.

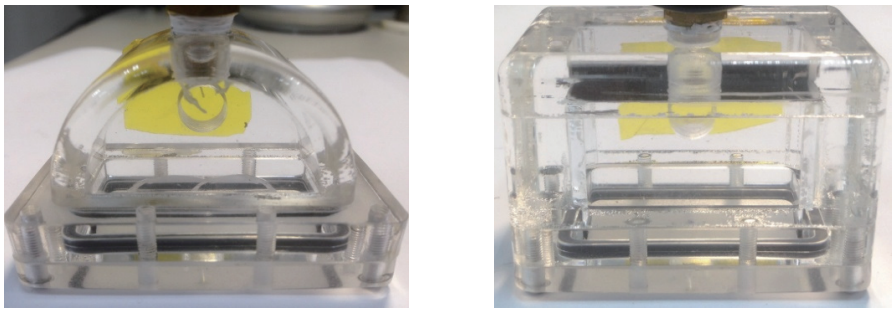

(a) (b)

Fig. 7. (Color online) Appearance of devices with (a) hemicylindrical chamber and (b) rectangular chamber.

Fig. 8. (Color online) Heater wire and thermal sensors (K-type thermocouples) were fixed on engineering PI tape.

### 3.2 Results of test

In this section, the separation distance $D$ was varied as 2, 4, 6, and 8 mm. Figures 10 and 11 show the sensitivity curves (using hemicylindrical and rectangular chambers filled with air and no stacked layer) of the simulation results, respectively. The reason for filling the chambers with air and not using a stacked layer was to enable easy implementation. Note that the sensitivities were indeed better when using a hemicylindrical chamber. Moreover, the sensitivities were always high with the lowest $D$ (= 2 mm), as previously discussed. Note that drooping effects also appeared at larger inclination angles in both figures, because the stacked layers were not applied under the thermal sensors for convenience. Also, note that there were some differences between those curves obtained for the practical devices and the simulated curves, as shown in Figs. 12 and 13, because two K-type thermocouples were applied in the practical devices instead of the thermal sensors using the p-type semiconductor adopted in the simulation.

On the other hand, the results in Figs. 12 and 13 were examined to compare the performances of the practical device and the simulation model with hemicylindrical and rectangular chambers. The results for the prototype device and the simulation model were labeled as $I$ and $S$, respectively. Note that the sensitivities for $D$ = 2 mm were the best when using the hemicylindrical chamber in the practical device.

Also, note that there were some differences between the curves for the practical device and the simulation results in Figs. 12 and 13, because two K-type thermocouples were applied in the practical device instead of the thermal sensors with p-type semiconductor in the simulation.

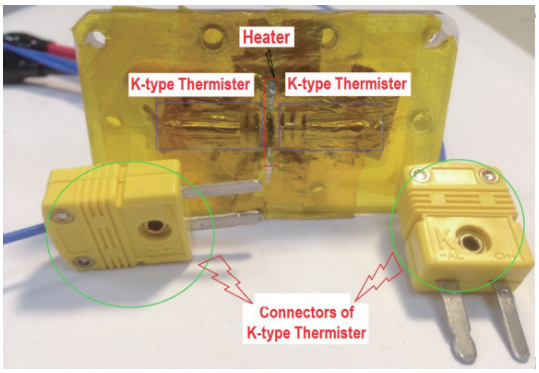


Fig. 9. (Color online) Proposed inclinometer with heater wire and K-type thermocouples fixed on PI tape.

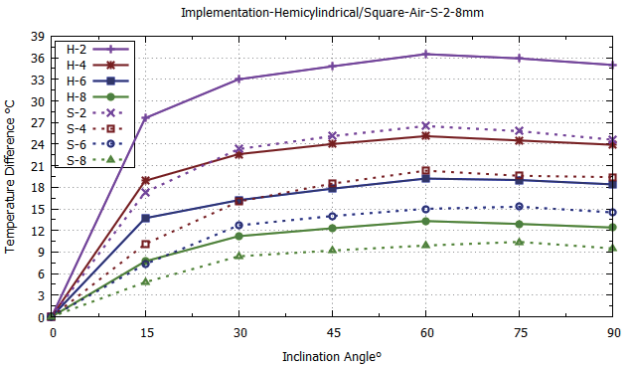


Fig. 10. (Color online) Sensitivity curves of inclinometers using rectangular and hemicylindrical chambers with different *S* values (2, 4, 6, and 8 mm).

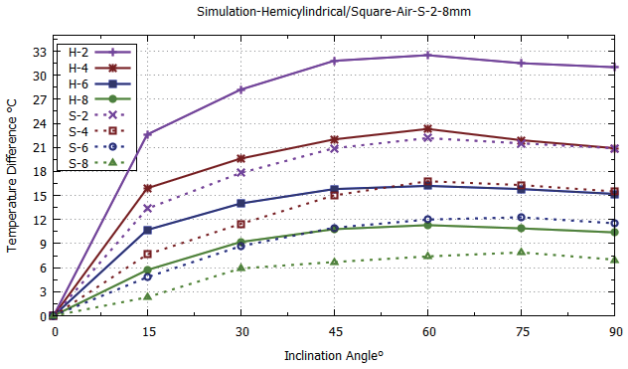


Fig. 11. (Color online) Simulation results of sensitivity curves for rectangular and hemicylindrical chambers with different *D* values (2, 4, 6, and 8 mm).

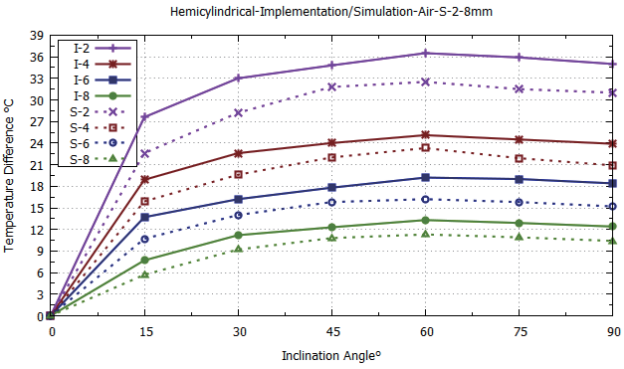


Fig. 12. (Color online) Sensitivity curves with air in a hemicylindrical chamber of a practical device and simulation results.

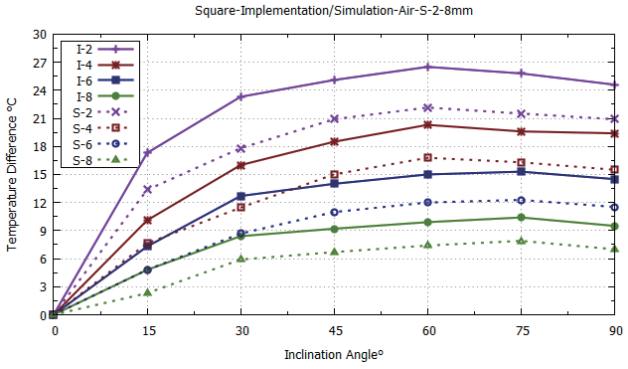


Fig. 13. (Color online) Sensitivity curves with air in a rectangular chamber for a practical device and simulation results.

Furthermore, the practical devices were roughly made in our lab merely to show the proposed new ideas and functions for the purpose of demonstration. The photolithography resolution was not very high and the fabrication processes were not finely tuned, thus the output response curves shown in Figs. 5 and 6 exhibited some variations and fluctuations. However, the proposed new ideas and functions were verified to satisfy the intended purpose. If the devices are precisely fabricated using well-developed semiconductor or MEMS fabs, the performances would be better.

## 4. Conclusions

A novel thermal convection inclinometer was proposed by fixing a hemicylindrical chamber on a flexible substrate (such as PI tape) instead of the traditional rectangular chamber on a silicon wafer. Furthermore, the heater and thermal sensors were implemented directly on the flexible substrate instead of over a cavity on the silicon substrate. Therefore, the cost can be considerably reduced and the device will be more reliable. Moreover, inert xenon gas instead of the previous $CO_2$ was used to fill the chamber to avoid the oxidation effect for both the heater and thermal sensors. In this work, we also performed a study in which the separation distance between the components and the thickness of the stacking material of aluminum nitride were varied to determine their effects.

## Acknowledgments

This work was supported by the Ministry of Science and Technology in Taiwan under grant No. MOST 105-2622-E- 216-005-CC2.

## References

1 J. M. Lin and C. H. Lin: Proc. Int. Conf. Computer, Networks and Communication Engineering, Beijing, China (2013) 569.
2 F. Khoshnoud and C. W. de Silva: IEEE Instrum. Meas. Mag. **15** (2012) 14.
3 A. Garraud, A. Giani, P. Combette, B. Charlot, and M. Richard: Sens. Actuators, A **170** (2011) 44.
4 Y. Zhao, A. P. Brokaw, M. E. Rebeschini, A. M. Leung, G. P. Pucci, and A. Dribinsky: U.S. Patent No. 6795752 (2004).
5 Y. Zhao, A. Leung, M. E. Rebeschini, G. P. Pucci, A. Dribinsky, and Y. Cai: U.S. Patent No. 7305881 (2007).
6 A. Dribinsky, G. P. Pucci, Y. Cai, M. Varghese, and G. J. O'Brien: U.S. Patent No. 7862229 (2011).
7 B. Alain, A. Boyer, A. Renault, B. Varusio, and A. Giani: European Patent No. 1550874 (2010).
8 G. Piazza and P. Stephanou: J. Microelectromech. Syst. **15** (2006) 1406.
9 J. Bahari and A. M. Leung: J. Micromech. Microeng. **21** (2011) 1.
10 J. Courteaud, N. Crespy, P. Combette, B. Sorli, and A. Giani: Sens. Actuators, A **147** (2008) 75.
11 J. Dido, P. Loisel, and A. Renault: U.S. Patent No. 7426862 (2008).
12 K. M. Liao, R. Chen, and B. C. S. Chou: Sens. Actuators, A **130**–**131** (2006) 282.
13 L. Lin, R. T. Howe, and A. P. Pisano: J. Microelectromech. Syst. **7** (1998) 286.
14 L. C. Spangler and C. J. Kemp: Sens. Actuators, A **54** (1996) 523.
15 A. Petropoulosa, A. Moschosa, S. Athineosa, and G. A. Kaltsas: Procedia Eng. **25** (2011) 643.
16 R. Dao, D. E. Morgan, H. H. Kries, and D. M. Bachelder: U.S. Patent No. 5581034 (1996).
17 A. A. Rekik, F. Azaïs, N. Dumas, F. Mailly, and P. Nouet: J. Electron. Test. **27** (2011) 411.
18 T. Mineta, S. Kobayashi, Y. Watanabe, S. Kanauchi, I. Nakagawa, E. Suganuma, and M. Esashi: J. Micromech. Microeng. **6** (1996) 431.

19 U. A. Dauderstadt, P. H. S. de Vries, R. G. Hiratsuka, J. Korvink, P. M. Sarro, H. Baltes, and S. Middelhoek: Sens. Actuators, A **55** (1996) 3.
20 U. A. Dauderstadt, P. M. Sarro, and P. J. French: Sens. Actuators, A **66** (1998) 244.
21 X. B. Luo, Z. X. Li, Z. Y. Guo, and Y. J. Yang: J. Micromech. Microeng. **11** (2001) 504.

## About the Authors

**Jium-Ming Lin** graduated from the Deptartment of Electronic Engineering, National Chiao-Tung University, Taiwan, in 1974. He received his Master's and Ph.D. degrees from the Institute of Electronics of the same university in 1976 and 1985, respectively. He became an adjunct professor and then a full professor in 1992 and 1996, respectively, of the Department of Mechanical Engineering, Chung-Hua University, Taiwan. At present, he is a distinguished professor with the Deptartment of Electronic Engineering, and specializes in RFID; accelerometer; rate gyro; multivariable, optimal, stochastic, and fuzzy-neural control; avionics; and MEMS. He also has many patents in related areas.

**Cheng-Hung Lin** graduated from the Department of Mechanical Engineering, Chung-Hua University at Hsin-Chu, Taiwan, in 2009. He received his Master's degree from the same university in 2012. His major fields are in navigation, guidance and control. His other interests are in RFID, wireless accelerometer and rate gyro, multivariable control, optimal control, stochastic control, fuzzy-neural control, avionics, and MEMS design. He is a Ph.D. candidate in the Program of Engineering Science, College of Engineering, Chung-Hua University.